



Article

TiO₂ Nanostructured Films for Electrochromic Paper Based-Devices

Daniela Nunes ^{1,*} , Tomas Freire ¹, Andrea Barranger ¹, João Vieira ¹ , Mariana Matias ¹,
Sonia Pereira ¹, Ana Pimentel ¹, Neusmar J. A. Cordeiro ^{1,2}, Elvira Fortunato ¹ and
Rodrigo Martins ^{1,*}

¹ i3N/CENIMAT, Department of Materials Science, Faculty of Sciences and Technology, Universidade NOVA de Lisboa and CEMOP/UNINOVA, 2829-516 Campus de Caparica, Caparica, Portugal; tm.freire@campus.fct.unl.pt (T.F.); andreabarranger53@gmail.com (A.B.); jpc.vieira@campus.fct.unl.pt (J.V.); ms.matias@campus.fct.unl.pt (M.M.); sp@uninova.pt (S.P.); acgp@campus.fct.unl.pt (A.P.); Neusmar.jr@gmail.com (N.J.A.C.); emf@fct.unl.pt (E.F.)

² Physics Department, Londrina State University, Rodovia Celso Garcia Cid, PR 445, km 380, Londrina 86057-970, Brazil

* Correspondence: daniela.gomes@fct.unl.pt (D.N.); rm@uninova.pt (R.M.)

Received: 15 January 2020; Accepted: 7 February 2020; Published: 11 February 2020



Abstract: Electrochromic titanium dioxide (TiO₂) nanostructured films were grown on gold coated papers using a microwave-assisted hydrothermal method at low temperature (80 °C). Uniform nanostructured films fully covered the paper substrate, while maintaining its flexibility. Three acids, i.e., acetic, hydrochloric and nitric acids, were tested during syntheses, which determined the final structure of the produced films, and consequently their electrochromic behavior. The structural characteristics of nanostructured films were correlated with electrochemical response and reflectance modulation when immersed in 1 M LiClO₄-PC (lithium perchlorate with propylene carbonate) electrolyte, nevertheless the material synthesized with nitric acid resulted in highly porous anatase films with enhanced electrochromic performance. The TiO₂ films revealed a notable contrast behavior, reaching for the nitric-based film optical modulations of 57%, 9% and 22% between colored and bleached states, at 250, 550 and 850 nm, respectively in reflectance mode. High cycling stability was also obtained performing up to 1500 cycles without significant loss of the electrochromic behavior for the nitric acid material. The approach developed in this work proves the high stability and durability of such devices, together with the use of paper as substrate that aggregates the environmentally friendly, lightweight, flexibility and recyclability characters of the substrate to the microwave synthesis features, i.e., simplicity, celerity and enhanced efficiency/cost balance.

Keywords: TiO₂ nanostructured films; paper substrates; microwave irradiation; electrochromic stability and durability

1. Introduction

Titanium dioxide (TiO₂) is a versatile material being investigated for applications ranging from photocatalysis [1–5], dye-solar cells [6,7], sensors [8–11] to electrochromic devices (EC) [12–14]. In recent years, the use of TiO₂ integrated on electrochromic devices has been increasing exponentially [15–18], also in association with tungsten oxide (WO₃), which is the most widely studied electrochromic material [19–24].

A material is considered electrochromic when a reversible change on its optical properties (transmittance and reflectance) associated with an electrochemically induced oxidation-reduction reaction occurs under an applied voltage or current [25]. In that case, TiO₂ appears as an appealing

electro-active material due to its intrinsic characteristics, such as high EC activity, strong oxidation capability and enhanced chemical stability [26]. Moreover, TiO₂ has a wide band gap (3.00 and 3.21 eV for rutile and anatase, respectively [27], and from 3.13 to 3.40 eV [27,28] for brookite) and presents a lattice structure that easily allows cation intercalation. This intercalation leads to additional electronic states in its bandgap causing the change in optical properties which results in light absorption in the visible range [15]. Indeed, TiO₂ in the form of anatase is considered the most promising material for electrochromic devices [14].

The EC materials are largely integrated in smart windows, displays and mirrors, however the demand for flexible devices has been gradually growing in the recent years, especially due to their conformability characteristic to unlike surfaces and the need to reduce production costs [29]. In this sense, electronics on paper appears as an attractive option as cellulose is the most abundant biopolymer on earth, inexpensive and guarantee highly flexibility to the device, despite being environmentally friendly [30]. In fact, paper has been included in several optoelectronic devices, including solar cells, transistors, among others [30,31], and lately paper started to appear as a reliable alternative for EC devices, as previously reported in [30,32–34].

The production route of the electro-active materials is a key factor on the final cost of the EC device, moreover the production route selected must be in line with the limitations of the substrates. Several techniques have been reported to produce TiO₂ EC films, including magnetron sputtering [35], spin-coating [36] and sol-gel methods [37], hydrothermal synthesis [14], and microwave synthesis [38]. This latter synthesis route is compatible with flexible substrates [3,39] and paper electronics [40], and it is reliable, inexpensive, simple and rapid. Moreover, the microwave synthesis guarantee precisely the control of synthesis parameters [41], and thus the produced material homogeneity and uniformity. In fact, the structure of the electro-active materials largely influences the final EC device performance, where nanostructured or nanoporous films are desired [13].

The present study reports the synthesis and characterization of TiO₂ nanostructured films using paper as substrate, and produced with a hydrothermal method assisted by microwave irradiation. Low temperature synthesis was employed (80 °C) and the materials were tested as EC devices. The main goal is to produce TiO₂ electrochromic nanostructured films with low-cost synthesis routes but also the fabrication of highly electro-active, stable, flexible, environmentally friendly, and cost effective EC devices. Moreover, to the best of the author's knowledge, TiO₂ nanostructured films grown with a microwave-assisted hydrothermal method and having gold coated-paper substrates to be employed as EC devices has never been reported before. Structural characterization of the TiO₂ nanostructured films has been carried out by scanning electron microscopy (SEM) coupled with focused ion beam (FIB) and X-ray energy dispersive spectroscopy (EDS), and by Raman spectroscopy.

2. Experimental Details

2.1. Synthesis of TiO₂ Films and Gold Deposition

Hydrothermal synthesis assisted by microwave irradiation has been used for the production of the TiO₂ nanostructured films. For the TiO₂ microwave synthesis, it has been used deionised water, titanium (IV) isopropoxide (Ti[OCH(CH₃)₂]₄, TTIP, 97% from Sigma Aldrich), and three types of acid, i.e. nitric acid (HNO₃, 65%), hydrochloric acid (HCl, 37%) and acetic acid glacial (CH₃COOH, 99%). In each synthesis, 55 mL of water was added to 5 mL of each acid and stirred for 5 min. Then, 2 mL of TTIP was mixed, leaving the final solution under stirring for 10 min before synthesis.

Whatman chromatography paper grade two was used as substrate. This pure cellulose paper has been selected due to the lack of impurities or additives present together with its uniformly absorbent properties [42,43]. Prior to synthesis, the paper substrate was subjected to the conductive layer deposition. At this point, a gold film of 140 nm was deposited by e-beam evaporation in a homemade system and at room temperature. Gold is the most common thin-film conductor material, however its electrical properties are largely influenced by several parameters including the substrate used [44]. One

important parameter that influences the EC performance is the sheet resistance of the contact, in fact the decrease of the sheet resistance has been reported to accelerate switching speeds of the EC devices [45]. Nevertheless, in the present study, the deposition parameters have been systematically maintained and highly reproducible thin films have been obtained, so the influence of Au sheet resistance is expected to be equivalent for all the devices produced.

Any seed layer has been used for assisting the TiO₂ growth [10,43]. Afterwards, the gold coated paper substrate was cut (30.0 × 15.0 mm) and prepared for synthesis. A part of the substrate was covered on its edge (5.0 × 15.0 mm) to prevent the deposition of the TiO₂ film on the conductive layer (Figure 1). The novel approach developed to protect the Au contacts was imperative to maintain the conductive character of the inner contact.

Microwave synthesis was carried out using a CEM Focused Microwave Synthesis System Discover SP. Time, power, temperature and pressure have been set at 120 min, 100 W, 80 °C and 200 Psi, respectively. Then 20 mL of the final solutions were transferred into capped quartz vessels of 35 mL, which were maintained sealed during the entire reaction. In the microwave vessel, a piece of the gold coated substrate was placed at an angle against it, with gold facing down.

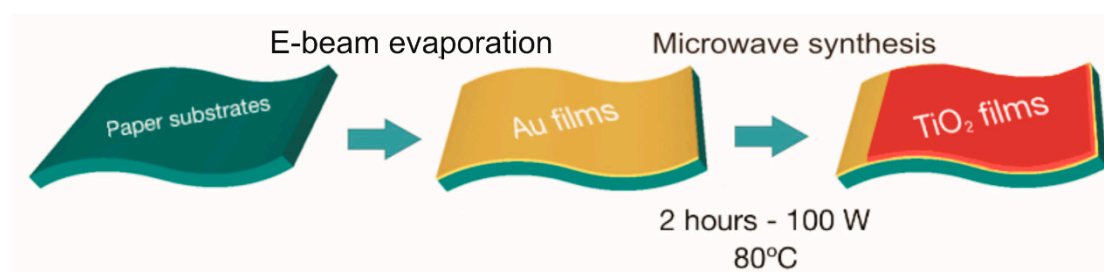


Figure 1. Scheme of the gold layer deposition followed by the titanium dioxide (TiO₂) nanostructured film growth under microwave irradiation.

2.2. Characterization Techniques

X-ray diffraction measurements were carried out using a PANalytical's X'Pert PRO MPD diffractometer equipped with a X'Celerator 1D detector and using CuK α radiation. The XRD diffractograms were obtained in the 20–45° 2 θ range with a step size of 0.05°. The powder diffractograms of rutile, anatase, brookite were simulated with PowderCell [46] using crystallographic data from reference [47] for comparison.

Raman spectroscopy experiments were performed with an inVia Qontor confocal Raman microscope from Renishaw. The measurements were obtained with a 17 mW He–Ne laser operating at 532 nm. Surface and cross-section SEM observations were carried out using a Carl Zeiss AURIGA CrossBeam FIB-SEM workstation equipped for EDS and FIB measurements. The FIB experiments were performed to observe the thickness of the TiO₂ films. The Ga⁺ ions were accelerated to 30 kV at 20 pA and the etching depth was kept around 1 μ m. The dimensions of individual nanoparticles and films have been determined from SEM micrographs using ImageJ software [48].

2.3. Electrochromic Measurements

The TiO₂ nanostructured films had their electrochromic behavior investigated by cyclic voltammetry (CV) on a potentiostat (Gamry reference 600). All materials were electrochemically cycled in 1 M LiClO₄–PC, at a scan rate of 500 mV/s, in a three-electrode arrangement, with Au paper with the TiO₂ nanostructured films as the working electrode, platinum wire as counter electrode and Ag/AgCl as the reference electrode. It has been applied a voltage of –5 V and 5 V. The higher applied potential window tested in this study is associated to the porous substrate used.

The optical reflectance between 200 and 800 nm was measured using a UV–VIS–NIR spectrophotometer (SPEC STD UV/Vis, Sarspec, Vila Nova de Gaia, Portugal). For calibration, the measurements were performed considering the Au paper with the TiO₂ nanostructured films plus

the electrolyte (1 M LiClO₄-PC) as 100%. The in-situ reflectance changes of the TiO₂ electrochromic films were measured with the same spectrophotometer combined with the potentiostat at a wavelength of 550 nm, applying a voltage of -5 V and 5 V. The samples were immersed in the electrolyte contained in a glass cell, using a platinum wire as counter electrode.

3. Results and Discussion

TiO₂ nanostructured films were synthesized using a microwave-assisted hydrothermal method and having paper as substrate with gold contacts to be used as electrochromic flexible devices. The syntheses were carried out using different acids, at low temperatures and without any seed layer. The TiO₂ nanostructured films and final devices were systematically investigated including their electrochromic behaviors.

3.1. Structural Characterization

Figure 2 depicts the SEM images of pristine Au paper together with the TiO₂ nanostructured films. As observed in analogous studies [10,43], the TiO₂ nanostructured films were grown on the cellulose-based substrate without any seed layer and directly on the Au contact. It has been previously stated that the paper roughness facilitates nucleation and fixation of the TiO₂ nanostructures [10]. The structure of the deposited Au film is presented in Figure 2a, and no similarity to the TiO₂ films could be observed. The Au contacts appear as a uniform and homogeneous layer, without any visible porosity. The cellulose fibers of the Whatman paper could be observed after microwave synthesis, however with the magnified SEM image, it is clear that the substrates were uniformly covered, forming continuous TiO₂ nanostructured films. Moreover, the structural differences observed comparing the acids are evident. The TiO₂ film synthesized with nitric acid is composed by densely and closely packed nanoparticles joined to form spherical-like structures nanoaggregates, with ~30 nm of mean diameter (Figure 2b). From the cross-section, it can be seen that the nitric-based film is highly porous, with film thickness around 350 nm. When it turns to the hydrochromic-based TiO₂ film (Figure 2c), it can be observed a rougher overall structure, but formed by fine densely agglomerated nanoparticles (~10 nm). From FIB measurements, it could also be observed nanoporosity, with a film thickness of 200 nm. In the case of the acetic acid, a compact and homogeneous film could be observed after synthesis. The nanostructured film was composed by nanoparticles with sizes around 10 nm, and thickness varying from 300 to 500 nm. Low porosity could be observed from the cross-section, in fact the acetic film revealed to be thicker than the other materials synthesized (Figure 2d). The expressive structure differences observed regarding the acid used are expected to be related to the microwave synthesis path. Figure S1 shows the microwave pressure profile associated to the acid used. It is clear the synthesis using nitric acid reached highest pressure values throughout the synthesis, followed by hydrochloric acid and then acetic acid. The microwave pressure/temperature relation to the outcome of nanoparticles has been previously reported. Li et al. [49] suggested the direct effect of applying higher microwave synthesis pressure to the morphology and size of the nanomaterials. It has been also demonstrated the influence of the solvent used during syntheses and the final synthesis temperature/pressure with a direct effect on the nanoparticle structure [39,50]. These effects are related to the microwave interactions to the reagents or precursors, and solution medium, that will influence the nucleation and crystallization rates [51].

EDS analyses were carried out on all films synthesized, confirming the homogeneous distribution of Ti along the substrates (Figure 3). Au comes from the contacts deposited, and no other impurities were detected. The significant presence of C and O is also related to the Whatman paper substrate used [43]. Moreover, it has been noticed that the Ti EDS map is more intense for the acetic-based film, with is expectable since this is the thicker film synthesized (Figure 3l).

Raman spectroscopy and X-Ray diffraction measurements were carried out for the TiO₂ nanostructured films together with the pristine Au paper. A considerable contribution from the substrate was observed on XRD diffractograms, hindering the TiO₂ signal (Figure 4a). The XRD

characteristic peaks of native cellulosic fibers are clearly observed at 22.7° and 35° , in agreement to the literature [43,52]. Nevertheless, at $\sim 25^\circ$, a slightly peak was detected, which can be associated to the presence of anatase. Raman spectroscopy was able to overcome the XRD limitation, allowing the precise identification of the TiO_2 phases present [53] (Figure 4b). The pristine Au paper Raman spectrum is presented for comparison, and no contribution was detected. Raman spectra were recorded in the range of $100\text{--}700\text{ cm}^{-1}$ and confirmed the presence of anatase phase. The Raman bands associated to anatase can be assigned to 155 cm^{-1} (E_g), 205 cm^{-1} (E_g), 397 cm^{-1} (B_{1g}), 510 cm^{-1} ($B_{1g} + A_{1g}$), and 636 cm^{-1} (E_g) for anatase [54–56]. This Raman band shift observed can be associated to the presence of structural defects in the TiO_2 lattice [57] or minor deviations from stoichiometry of the TiO_2 films [58]. Moreover, the smooth aspect of the TiO_2 thin film spectra has been reported before [57,58], and detected especially for the films synthesized with nitric and hydrochloric acids.

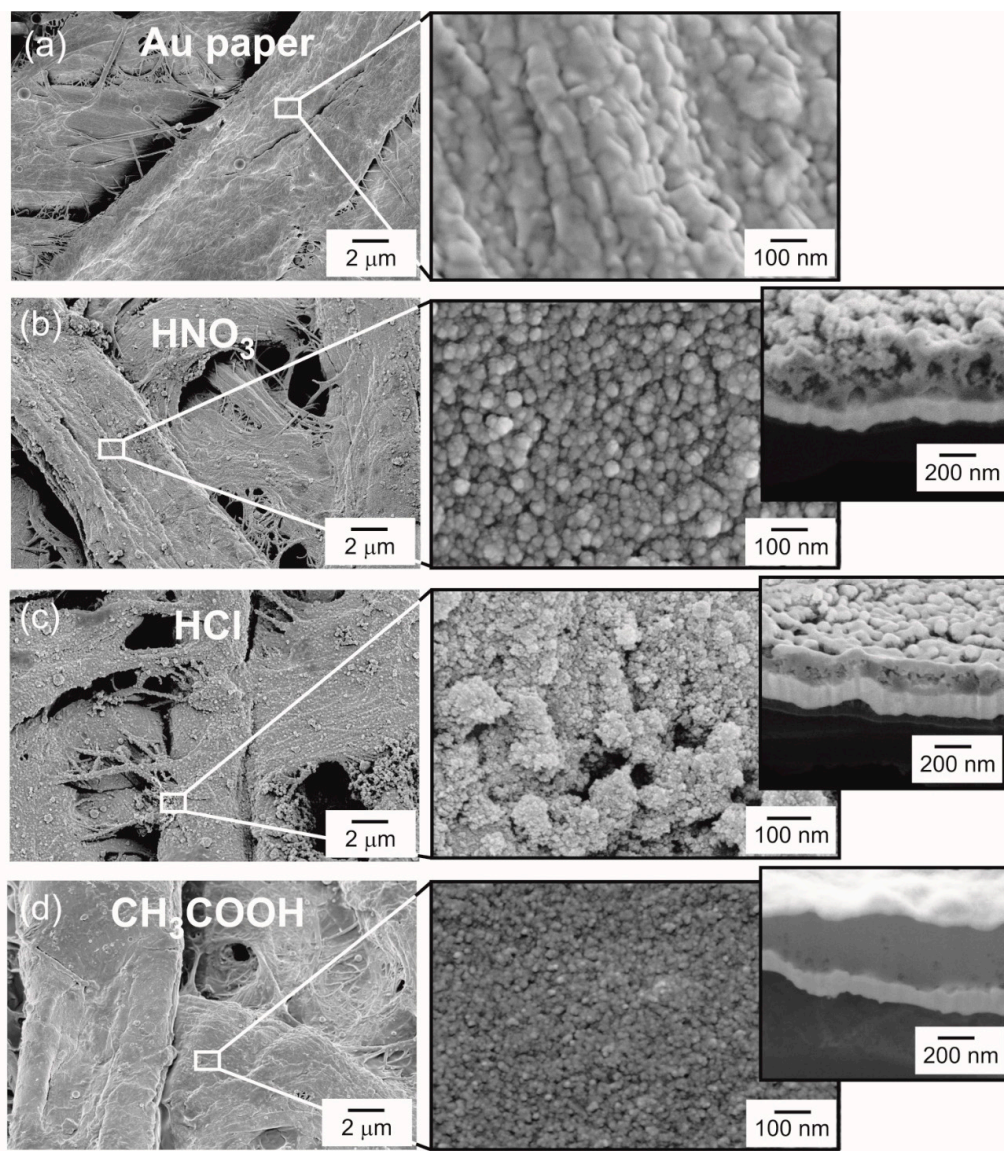


Figure 2. SEM images showing the Whatman paper with an Au film and the TiO_2 nanostructured films grown under microwave irradiation. (a) Whatman paper with a 140 nm Au film deposited by ebeam to act as contact. (b) Synthesis of the TiO_2 nanostructured films using nitric acid, (c) hydrochloric acid, and (d) acetic acid. The insets demonstrate the TiO_2 film thicknesses. An Au/Pd sacrificial layer has been deposited on the top of the TiO_2 films.

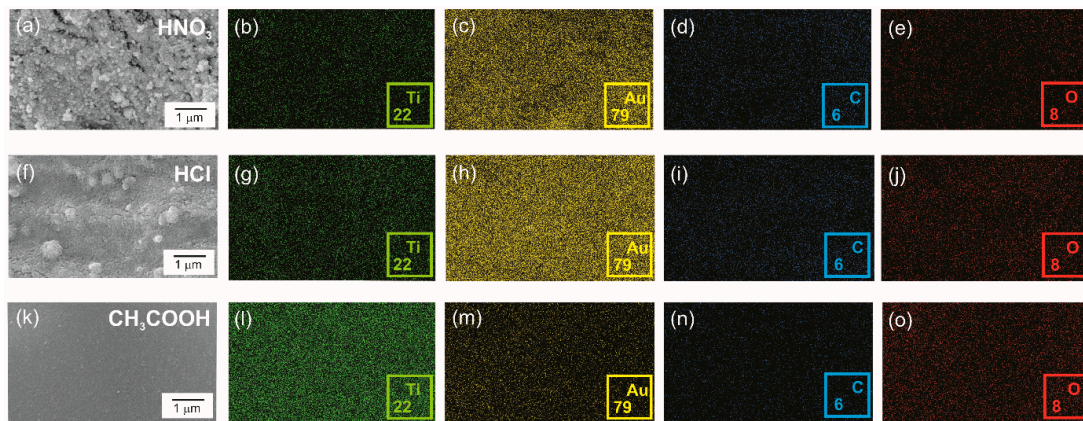


Figure 3. SEM images of the TiO₂ nanostructured films produced using nitric acid (a), hydrochloric acid (f) and acetic acid (k) together with their corresponding energy dispersive spectroscopy (EDS) maps of Ti, (b,g,l), Au (c,h,m), C (d,i,n) and O (e,j,o).

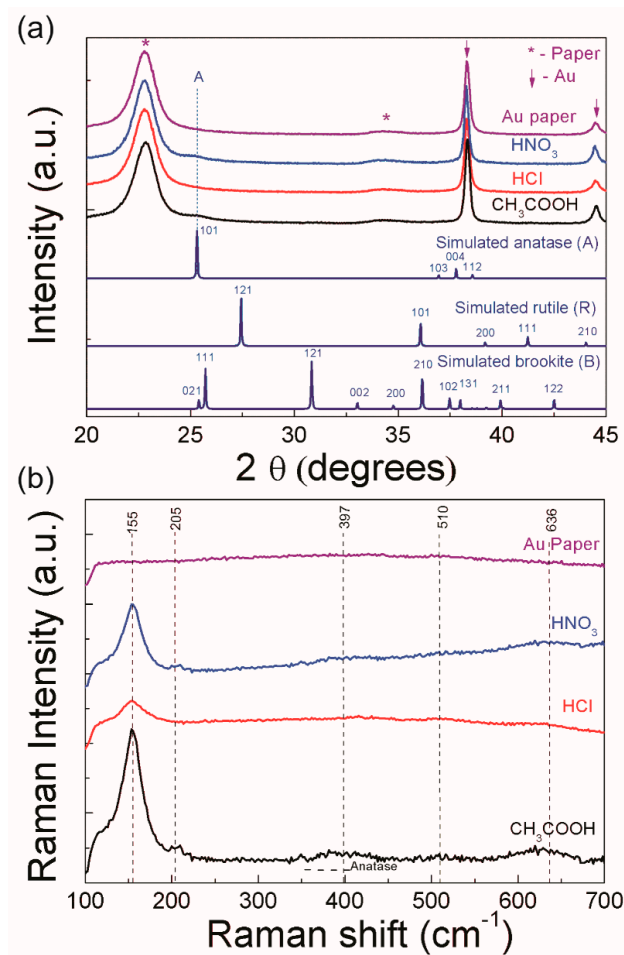


Figure 4. (a) XRD diffractograms of the TiO₂ nanostructured films grown on Au paper together with the pristine Au paper. For comparison, the simulated XRD diffractograms of rutile, brookite and anatase are presented. (b) Raman spectra of the nanostructured films and the pristine Au paper. Dashed lines indicate the anatase bands.

3.2. Electrochromic and Electrochemical Behavior

The electrochromic behavior of the TiO₂ nanostructured films grown on Au paper with different acids was investigated by measuring the reflectance variation between 200 to 800 nm. In order to get comparable results, the same active area (1 cm²) was defined for all EC devices. Figure 5 shows the data obtained after several coloration/bleaching cycles up a maximum of 1500 in 1 M LiClO₄-PC and applying ±5 V in order to stabilize the redox reactions. The insertion/deinsertion of Li⁺ in the TiO₂ nanostructured films is accompanied by a color change. The TiO₂ nanostructured films change from dark blue, at the colored state, to transparent appearing the yellow coloration from the Au contact color, at the bleached state. The optical modulations of TiO₂ films between colored and bleached states were: 57%, 9% and 22%, at 250, 550 and 800 nm, respectively, for the nitric-based material, while the hydrochloric film, it presented 13%, 8% and 20% at 250, 550 and 800 nm, respectively. The acetic-based TiO₂ film, reached optical modulations of 10%, 3%, and 12% at 250, 550 and 800 nm, respectively. The increase of reflectance in the IR region has been reported previously for TiO₂ [59]. The highest optical modulation was achieved for the nitric-based film, demonstrating a good contrast behavior with deep color change, as can be seen on Figure 5a. The enhanced electrochromic performance observed for the TiO₂ film synthesized with nitric acid is expected to be related to the high porosity observed (Figure 2b). The higher EC performance with porous materials have been reported previously [60,61], and it has been attributed to the increment in charge density incorporated into porous layers (easier electrolyte penetration and Li⁺ diffusion) during the oxidation and reduction reactions [60,61]. The TiO₂ film synthesized using hydrochloric acid also demonstrated the presence of porosity in its structure, however due to its lower thickness, it is expected a poorest EC performance when compared to nitric since thin layers are known to have less active mass [62]. The compact structure of the acetic-based TiO₂ film is thought to be responsible for the worst EC performance observed.

The reflectance measurements also demonstrate the high durability of the EC device produced with TiO₂ nanostructured films on paper substrates. As it has been previously said, to the author's best knowledge, it has never been reported a fully flexible EC device using TiO₂ on paper, and Figure 5 shows that this kind of substrates are reliable for at least 1500 cycles using a liquid electrolyte.

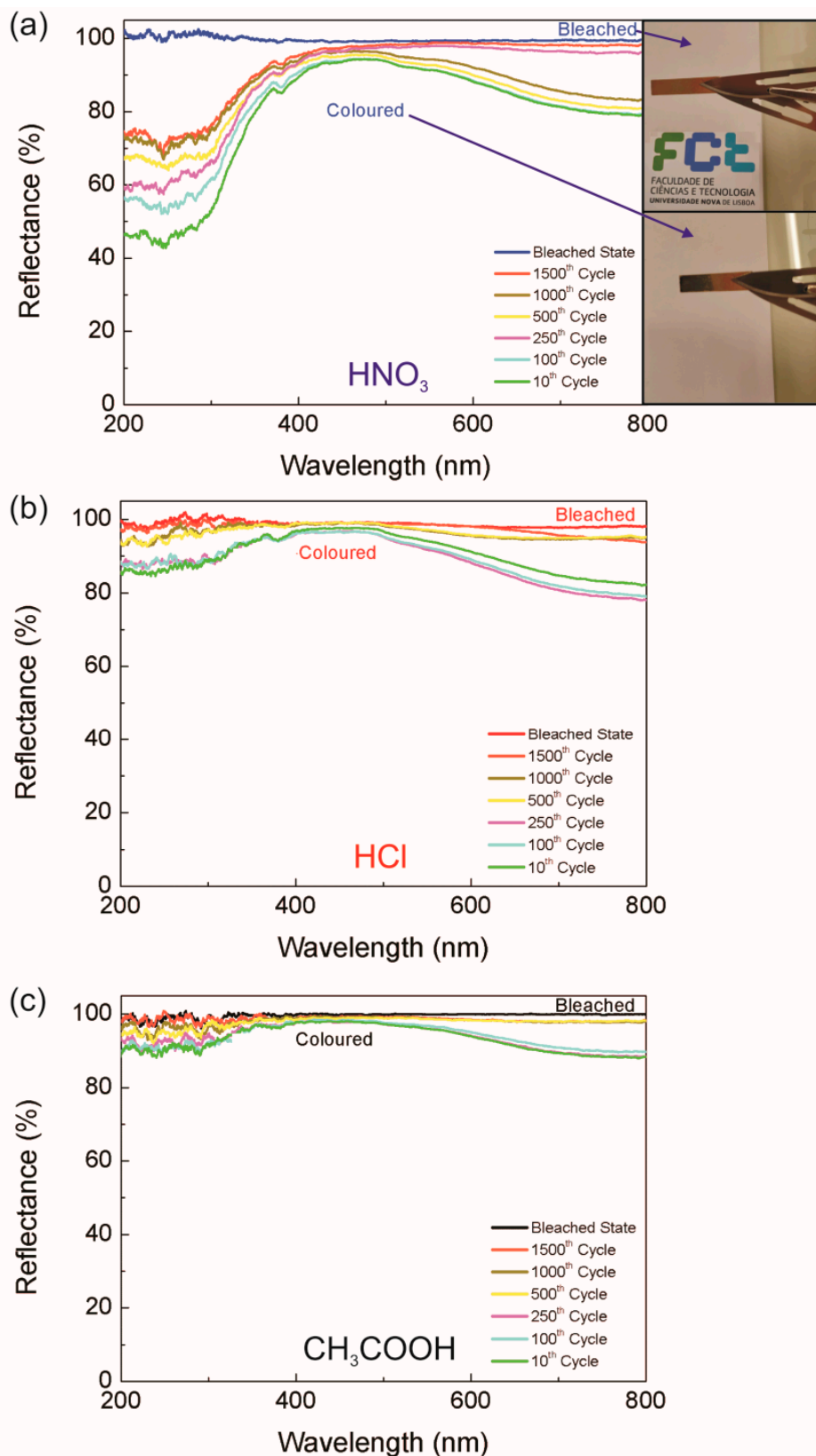


Figure 5. Reflectance spectra of the TiO₂ nanostructured films for colored and bleached states obtained after 10, 100, 250, 500, 1000 and 1500 coloration/bleaching cycles, applying ± 5 V. The bleached spectra presented was measured after 250 cycles. The results for TiO₂ nanostructured films synthesized using nitric acid are presented in (a), hydrochloric acid in (b), and acetic acid in (c). It also presented an image of the nitric-based TiO₂ film on the colored and bleached states carried out at room temperature.

As previously described, the TiO₂ coloration into dark blue is associated to the intercalation of Li⁺ in TiO₂. Thus, it is assumed that Li⁺ insertion/extraction is responsible for the gradual optical change of the TiO₂ nanostructured films, and so applying a negative potential causes the rapid accumulation of electrons on the TiO₂, which is compensated by small ions located close to the TiO₂-electrolyte interface. The proposed mechanism is suggested to be based on the formation of Ti³⁺ ions and the presence of the electrons in the conduction band [63]. The coloration state is attributed to the formation of the compound Li_xTiO₂ according to the cathodic Equation (1) [63,64]:



where x is the total of Li⁺ intercalation and e⁻ represents the charge-compensating electrons [65].

Cyclic voltammetry measurements were carried out for all the TiO₂ nanostructured films synthesized (Figure 6). Moreover, in Figure S2, it is presented all the voltammograms (1500 cycles) obtained during the CV experiments for the three types of TiO₂ films studied. The films' anodic scan oxidation leads to the bleaching state, and the cathodic scan reduction is associated to their coloring states. The nitric-based film demonstrated to be highly stable during cycles, maintaining the consistence during measurements without significant loss of its EC performance with the increase of the number cycles. In fact, the nitric-based material continued to work as an EC device after the cycles limit imposed (results not shown). In the cases of the hydrochloric and acetic-based films, it is clear that the EC performance has decreased with the increase of cycles, until the deficient EC device operation, with possible loss of optical modulation (Figure S2). Despite the increase in anodic and cathodic currents observed for the material synthesized with hydrochloric acid, its EC performance was substantially lower than the nitric one. Generally, the increase of anodic and cathodic currents indicates that the amount of ions and electrons inserted into the film also increases resulting in enhanced EC reaction activities [62], however, this effect has not been observed, as it can be seen by the instability observed on the CV voltammograms and lower durability of the device, with intercalation and deintercalation up to 850 cycles. The TiO₂ film synthesized with acetic acid demonstrated the poorest EC performance, reaching maximum of 800 cycles and lower currents (~±1 V), in agreement to what was observed in the optical measurements (Figure 5c).

The CV measurements attested the durability of TiO₂ nanostructured films, and as previously mentioned, the porous and thick structure of the nitric-based material guaranteed an improved EC performance, when compared with the other acids. Considering this, lifetime cycles measurements were carried out for this material (Figure 7). In order to stabilize the reflectance, the switching time was fixed at 240 s. The switching between both states was observed, with coloration of 71 s and bleaching times of 58 s, calculated as the time required to reach 10% to 90% of the initial and final reflectance values, respectively. Despite the long bleaching and coloring times, from the video presented in supplementary information, the visual color turning is faster than what was measured.

Other studies also reported the switch behavior of paper EC devices. Lang et al. [30] demonstrated EC devices with paper-based substrates and printed poly-(3,4-ethylenedioxythiophene):poly(styrenesulfonate) (PEDOT:PSS) electrodes showing slower switching time when produced with a lateral device architecture. Tehrani et al. [32] reported PEDOT:PSS-based EC displays with an extra layer of dihexyl-substituted poly(3,4-propylenedioxythiophene) (PProDOT-Hx2) and using flexible paper substrates in roll-to-roll printing. It has been demonstrated slow switch to the OFF-state of the produced devices, which was attributed to the poor ionic conductivity of the PProDOT-Hx2 film in the aqueous electrolyte. Taking in consideration paper-based UV sensors from an analogous study [10], the contribution from the paper structure shown to be imperative to the final performance of the electronic devices, so following this line, it can be suggested that a similar effect can occur with the EC devices.

Nevertheless, the low time response does not limit the utilization of such devices in every-day life, since it can be perfectly integrated in disposable sensors, such as in signaling devices, for one-time response. Moreover, the approach developed decreases the time of production and the fabrication cost of

related devices, since it joins the celerity and enhanced efficiency/cost balance of microwave synthesis to the inexpensive character of the cellulose-based substrate used. In fact, electronics on paper is proving to be an enabling technology for smart low-cost paper-based sensors, such as smart point-of-care biosensors and UV sensors, as photovoltaic devices [10,31,52], and as shown in this work, as electrochromic devices.

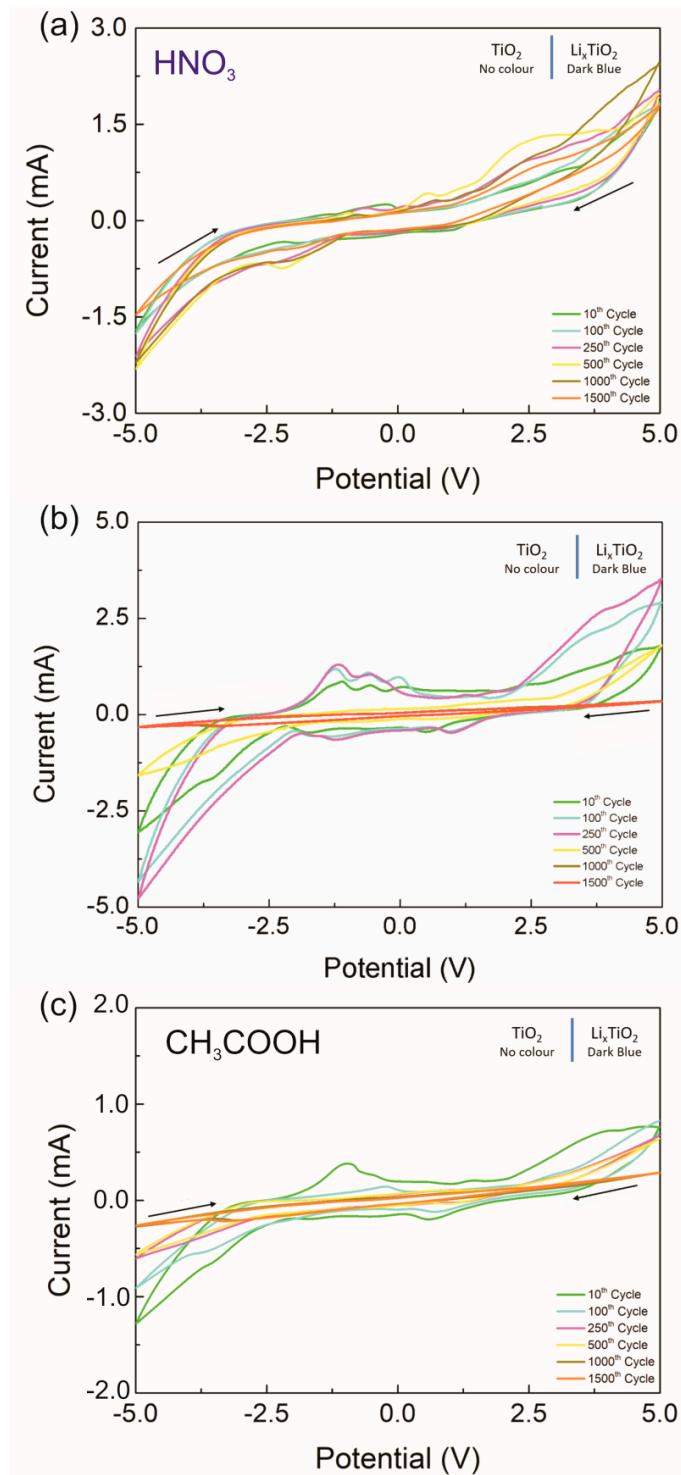


Figure 6. Cyclic voltammograms of TiO₂ nanostructured films from -5 V to 5 V (versus Ag/AgCl), at a scan rate of 500 mV/s, in a 1 M LiClO₄-PC electrolyte, after several cycles up to a maximum of 1500. Results for the TiO₂ nanostructured films synthesized using (a) nitric, (b) hydrochloric, and (c) acetic acids.

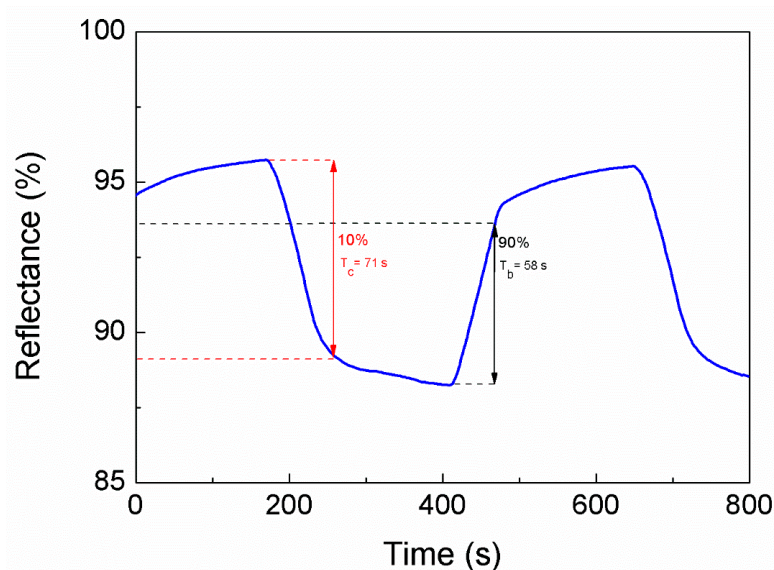


Figure 7. Lifetime cycles measurements for the TiO₂ nanostructured films synthesized using nitric acid, for applied voltages of -5 and 5 V (hold time of 240 s), with an exposed area of 1 cm^2 at 550 nm.

4. Conclusions

In this work, TiO₂ nanostructured films grown on paper substrate and using different acids were produced under microwave irradiation at low temperature ($80 \text{ }^\circ\text{C}$) to be employed as EC devices. The final structure of the produced films and their electrochromic behavior was deeply related to the acid used, with enhanced electrochromic performance for the film synthesized with acid nitric due to its higher thickness and highly porous nanostructure. In fact, nitric-based films resulted in EC devices with high cycling stability, without significant loss of their electrochromic behavior after 1500 cycles. The present work demonstrated that the simple approach developed is an effective and attractive alternative for producing flexible devices for several commercial applications, and due to the characteristics of the production techniques and substrates used, next-generation of green, one-time use and inexpensive EC devices with TiO₂ can be thought.

Supplementary Materials: The following are available online at <http://www.mdpi.com/2076-3417/10/4/1200/s1>, Figure S1: Microwave synthesis profiles for the different acids used. Figure S2: Cyclic voltammograms of TiO₂ nanostructured films from -5 V to 5 V (versus Ag/AgCl), at a scan rate of 500 mV/s , in a $1 \text{ M LiClO}_4\text{-PC}$ electrolyte, after several cycles up to a maximum of 1500. Results for the TiO₂ nanostructured films synthesized using (a) nitric, (b) hydrochloric. Video S1: Optical modulation of the paper-based TiO₂ nanostructured devices.

Author Contributions: T.F., A.B., J.V. and M.M. synthesized the materials and carried out the cyclic voltammetry measurements; D.N. and A.P. wrote the manuscript and performed the structural characterizations. S.P. and N.J.A.C. helped with the optical characterizations and interpretation of results; and the work and paper was under the supervision of R.M. and E.F. All authors have read and agreed to the published version of the manuscript.

Funding: This work was supported by FEDER funds, through the COMPETE 2020 Program, and national funds, through the Fundação para Ciência e Tecnologia (FCT), under the projects POCI-01-0145-FEDER-007688 (Reference UID/CTM/50025). The authors also acknowledge funding from the European Commission through the projects 1D-NEON (H2020-NMP-2015, grant 685758-21D), BET-EU (H2020-TWINN-2015, grant 692373) and DIGISMART (H2020 ERC AdG 787410). The work was also partially funded by the Nanomark collaborative project between INCM (Imprensa Nacional Casa da Moeda) and CENIMAT/i3N.

Conflicts of Interest: The authors declare no conflicts of interest.

References

1. Nakata, K.; Fujishima, A. TiO₂ photocatalysis: Design and applications. *J. Photochem. Photobiol. C Photochem. Rev.* **2012**, *13*, 169–189. [[CrossRef](#)]

2. Nunes, D.; Pimentel, A.; Pinto, J.V.; Calmeiro, T.R.; Nandy, S.; Barquinha, P.; Pereira, L.; Carvalho, P.A.; Fortunato, E.; Martins, R. Photocatalytic behavior of TiO₂ films synthesized by microwave irradiation. *Catal. Today* **2016**, *278*, 262–270. [[CrossRef](#)]
3. Nunes, D.; Pimentel, A.; Santos, L.; Barquinha, P.; Fortunato, E.; Martins, R. Photocatalytic TiO₂ nanorod spheres and arrays compatible with flexible applications. *Catalysts* **2017**, *7*, 60. [[CrossRef](#)]
4. Nunes, D.; Santos, L.; Pimentel, A.; Barquinha, P.; Pereira, L.; Fortunato, E.; Martins, R. *Metal Oxide Nanostructures: Synthesis, Properties and Applications*; Elsevier Science: Amsterdam, The Netherlands, 2018.
5. Schneider, J.; Matsuoka, M.; Takeuchi, M.; Zhang, J.; Horiuchi, Y.; Anpo, M.; Bahnemann, D.W. Understanding TiO₂ photocatalysis: Mechanisms and materials. *Chem. Rev.* **2014**, *114*, 9919–9986. [[CrossRef](#)] [[PubMed](#)]
6. Lin, J.; Heo, Y.-U.; Nattestad, A.; Sun, Z.; Wang, L.; Kim, J.H.; Dou, S.X. 3D hierarchical rutile TiO₂ and metal-free organic sensitizer producing dye-sensitized solar cells 8.6% conversion efficiency. *Sci. Rep.* **2014**, *4*, 5769. [[CrossRef](#)] [[PubMed](#)]
7. Park, N.-G.; van de Lagemaat, J.; Frank, A.J. Comparison of dye-sensitized rutile-and anatase-based TiO₂ solar cells. *J. Phys. Chem. B* **2000**, *104*, 8989–8994. [[CrossRef](#)]
8. Bernacka-Wojcik, I.; Senadeera, R.; Wojcik, P.J.; Silva, L.B.; Doria, G.; Baptista, P.; Aguas, H.; Fortunato, E.; Martins, R. Inkjet printed and “doctor blade” TiO₂ photodetectors for DNA biosensors. *Biosens. Bioelectron.* **2010**, *25*, 1229–1234. [[CrossRef](#)] [[PubMed](#)]
9. Bai, J.; Zhou, B. Titanium dioxide nanomaterials for sensor applications. *Chem. Rev.* **2014**, *114*, 10131–10176. [[CrossRef](#)] [[PubMed](#)]
10. Nunes, D.; Pimentel, A.; Araujo, A.; Calmeiro, T.; Panigrahi, S.; Pinto, J.; Barquinha, P.; Gama, M.; Fortunato, E.; Martins, R. Enhanced UV flexible photodetectors and photocatalysts based on TiO₂ nanoplateforms. *Topics Catal.* **2018**, *61*, 1591–1606. [[CrossRef](#)]
11. Nunes, D.; Pimentel, A.; Gonçalves, A.; Pereira, S.; Branquinho, R.; Barquinha, P.; Fortunato, E.; Martins, R. Metal oxide nanostructures for sensor applications. *Semicond. Sci. Technol.* **2019**, *34*, 043001. [[CrossRef](#)]
12. Diasanayake, M.A.K.L.; Senadeera, G.K.R.; Sarangika, H.N.M.; Ekanayake, P.M.P.C.; Thotawattage, C.A.; Divarathne, H.K.D.W.M.N.R.; Kumari, J.M.K.W. TiO₂ as a low cost, multi functional material. *Mater. Today Proc.* **2016**, *3*, S40–S47. [[CrossRef](#)]
13. Song, Y.-Y.; Gao, Z.-D.; Wang, J.-H.; Xia, X.-H.; Lynch, R. Multistage coloring electrochromic device based on TiO₂ nanotube arrays modified with WO₃ nanoparticles. *Adv. Funct. Mater.* **2011**, *21*, 1941–1946. [[CrossRef](#)]
14. Chen, J.-Z.; Ko, W.-Y.; Yen, Y.-C.; Chen, P.-H.; Lin, K.-J. Hydrothermally processed TiO₂ nanowire electrodes with antireflective and electrochromic properties. *ACS Nano* **2012**, *6*, 6633–6639. [[CrossRef](#)] [[PubMed](#)]
15. Ghicov, A.; Albu, S.P.; Macak, J.M.; Schmuki, P. High-contrast electrochromic switching using transparent lift-off layers of self-organized TiO₂ nanotubes. *Small* **2008**, *4*, 1063–1066. [[CrossRef](#)] [[PubMed](#)]
16. Chen, Y.; Bi, Z.; Li, X.; Xu, X.; Zhang, S.; Hu, X. High-coloration efficiency electrochromic device based on novel porous TiO₂@prussian blue core-shell nanostructures. *Electrochim. Acta* **2017**, *224*, 534–540. [[CrossRef](#)]
17. Patil, R.A.; Devan, R.S.; Liou, Y.; Ma, Y.-R. Efficient electrochromic smart windows of one-dimensional pure brookite TiO₂ nanoneedles. *Sol. Energy Mater. Sol. Cells* **2016**, *147*, 240–245. [[CrossRef](#)]
18. Berger, S.; Ghicov, A.; Nah, Y.C.; Schmuki, P. Transparent TiO₂ nanotube electrodes via thin layer anodization: Fabrication and use in electrochromic devices. *Langmuir* **2009**, *25*, 4841–4844. [[CrossRef](#)]
19. Cai, G.; Zhou, D.; Xiong, Q.; Zhang, J.; Wang, X.; Gu, C.; Tu, J. Efficient electrochromic materials based on TiO₂@WO₃ core/shell nanorod arrays. *Sol. Energy Mater. Sol. Cells* **2013**, *117*, 231–238. [[CrossRef](#)]
20. Nah, Y.-C.; Ghicov, A.; Kim, D.; Berger, S.; Schmuki, P. TiO₂-WO₃ composite nanotubes by alloy anodization: Growth and enhanced electrochromic properties. *J. Am. Chem. Soc.* **2008**, *130*, 16154–16155. [[CrossRef](#)]
21. Hashimoto, S.; Matsuoka, H. Prolonged lifetime of electrochromism of amorphous WO₃-TiO₂ thin films. *Surf. Interface Anal.* **1992**, *19*, 464–468. [[CrossRef](#)]
22. Reyes-Gil, K.R.; Stephens, Z.D.; Stavila, V.; Robinson, D.B. Composite WO₃/TiO₂ nanostructures for high electrochromic activity. *ACS Appl. Mater. Interfaces* **2015**, *7*, 2202–2213. [[CrossRef](#)] [[PubMed](#)]
23. Marques, A.; Santos, L.; Pereira, S.; Emanuele, U.; Sinopoli, S.; Igreja, R.; Sales, G.; Martins, R.; Fortunato, E. A planar electrochromic device using WO₃ nanoparticles and a modified paper-based electrolyte. *Proceedings* **2018**, *2*, 1065. [[CrossRef](#)]
24. Wojcik, P.J.; Cruz, A.S.; Santos, L.; Pereira, L.; Martins, R.; Fortunato, E. Microstructure control of dual-phase inkjet-printed a-WO₃/TiO₂/WO_x films for high-performance electrochromic applications. *J. Mater. Chem.* **2012**, *22*, 13268–13278. [[CrossRef](#)]

25. Wang, J.M.; Sun, X.W.; Jiao, Z. Application of nanostructures in electrochromic materials and devices: Recent progress. *Materials* **2010**, *3*, 5029–5053. [[CrossRef](#)] [[PubMed](#)]
26. Liu, S.; Zhang, X.; Sun, P.; Wang, C.; Wei, Y.; Liu, Y. Enhanced electrochromic properties of a TiO₂ nanowire array via decoration with anatase nanoparticles. *J. Mater. Chem. C* **2014**, *2*, 7891–7896. [[CrossRef](#)]
27. Reyes-Coronado, D.; Rodríguez-Gattorno, G.; Espinosa-Pesqueira, M.; Cab, C.; De Coss, R.; Oskam, G. Phase-pure TiO₂ nanoparticles: Anatase, brookite and rutile. *Nanotechnology* **2008**, *19*, 145605. [[CrossRef](#)]
28. Di Paola, A.; Bellardita, M.; Palmisano, L. Brookite, the least known TiO₂ photocatalyst. *Catalysts* **2013**, *3*, 36–73. [[CrossRef](#)]
29. Alesanco, Y.; Palenzuela, J.; Tena-Zaera, R.; Cabañero, G.; Grande, H.; Herbig, B.; Schmitt, A.; Schott, M.; Posset, U.; Guerfi, A.; et al. Plastic electrochromic devices based on viologen-modified TiO₂ films prepared at low temperature. *Sol. Energy Mater. Sol. Cells* **2016**, *157*, 624–635. [[CrossRef](#)]
30. Lang, A.W.; Österholm, A.M.; Reynolds, J.R. Paper-based electrochromic devices enabled by nanocellulose-coated substrates. *Adv. Funct. Mater.* **2019**, *29*, 1903487. [[CrossRef](#)]
31. Vicente, A.; Araujo, A.; Mendes, M.J.; Nunes, D.; Oliveira, M.J.; Sanchez-Sobrado, O.; Ferreira, M.P.; Aguas, H.; Fortunato, E.; Martins, R. Multifunctional cellulose-paper for light harvesting and smart sensing applications. *J. Mater. Chem. C* **2018**, *6*, 3143–3181. [[CrossRef](#)]
32. Tehrani, P.; Hennerdal, L.-O.; Dyer, A.L.; Reynolds, J.R.; Berggren, M. Improving the contrast of all-printed electrochromic polymer on paper displays. *J. Mater. Chem.* **2009**, *19*, 1799–1802. [[CrossRef](#)]
33. Monk, P.M.; Delage, F.; Vieira, S.M.C. Electrochromic paper: Utility of electrochromes incorporated in paper. *Electrochim. Acta* **2001**, *46*, 2195–2202. [[CrossRef](#)]
34. Brooke, R.; Edberg, J.; Crispin, X.; Berggren, M.; Engquist, I.; Jonsson, M.P. Greyscale and paper electrochromic polymer displays by UV patterning. *Polymers* **2019**, *11*, 267. [[CrossRef](#)] [[PubMed](#)]
35. Yoshimura, K.; Miki, T.; Tanemura, S. TiO₂ electrochromic thin films by reactive direct current magnetron sputtering. *J. Vac. Sci. Technol. A Vac. Surf. Films* **1997**, *15*, 2673–2676. [[CrossRef](#)]
36. Weng, W.; Higuchi, T.; Suzuki, M.; Fukuoka, T.; Shimomura, T.; Ono, M.; Radhakrishnan, L.; Wang, H.; Suzuki, N.; Oveisi, H. A high-speed passive-matrix electrochromic display using a mesoporous TiO₂ electrode with vertical porosity. *Angew. Chem. Int. Edit.* **2010**, *49*, 3956–3959. [[CrossRef](#)]
37. Dinh, N.N.; Oanh, N.T.T.; Long, P.D.; Bernard, M.C.; Hugot-Le Goff, A. Electrochromic properties of TiO₂ anatase thin films prepared by a dipping sol-gel method. *Thin Solid Films* **2003**, *423*, 70–76. [[CrossRef](#)]
38. Pillai, S.; McCormack, D.; Periyat, P.; Leyland, N.; Corr, D.; Colreavy, J. Rapid microwave synthesis of mesoporous TiO₂ for electrochromic displays. *J. Mater. Chem.* **2010**, *20*, 3650–3655.
39. Pimentel, A.; Nunes, D.; Pereira, S.; Martins, R.; Fortunato, E. Photocatalytic activity of TiO₂ nanostructured arrays prepared by microwave-assisted solvothermal method. In *Semiconductor Photocatalysis—Materials, Mechanisms and Applications*; InTech: Rijeka, Croatia, 2016.
40. Araujo, A.; Pimentel, A.; Oliveira, M.J.; Mendes, M.J.; Franco, R.; Fortunato, E.; Águas, H.; Martins, R. Direct growth of plasmonic nanorod forests on paper substrates for low-cost flexible 3D SERS platforms. *Flex. Print. Electron.* **2017**, *2*, 014001. [[CrossRef](#)]
41. Tsuji, M.; Hashimoto, M.; Nishizawa, Y.; Kubokawa, M.; Tsuji, T. Microwave-assisted synthesis of metallic nanostructures in solution. *Chem. A Eur. J.* **2005**, *11*, 440–452. [[CrossRef](#)]
42. Joubert, T.; Bezuidenhout, P.; Chen, H.; Smith, S.; Land, K. Inkjet-printed silver tracks on different paper substrates. *Mater. Today Proc.* **2015**, *2*, 3891–3900. [[CrossRef](#)]
43. Matias, M.L.; Nunes, D.; Pimentel, A.; Ferreira, S.H.; Agua, R.; Duarte, M.P.; Fortunato, E.; Martins, R. Paper-based nanoplatfoms for multifunctional applications. *J. Nanomater.* **2019**, *16*. [[CrossRef](#)]
44. Mingos, D.M.P.; Committee, A.S.M.I.H. *Electronic Materials Handbook: Packaging*; Taylor & Francis: Oxfordshire, UK, 1989.
45. Kim, K.-H.; Koo, B.-R.; Ahn, H.-J. Sheet resistance dependence of fluorine-doped tin oxide films for high-performance electrochromic devices. *Ceram. Int.* **2018**, *44*, 9408–9413. [[CrossRef](#)]
46. Kraus, W.; Nolze, G. POWDER CELL—A program for the representation and manipulation of crystal structures and calculation of the resulting X-ray powder patterns. *J. Appl. Crystallogr.* **1996**, *29*, 301–303. [[CrossRef](#)]
47. Pearson, W.B.; Villars, P.; Calvert, L.D. *Pearson's Handbook of Crystallographic Data for Intermetallic Phases*; American Society for Metals: Cleveland, OH, USA, 1985.

48. Schneider, C.A.; Rasband, W.S.; Eliceiri, K.W. NIH image to ImageJ: 25 years of image analysis. *Nat. Methods* **2012**, *9*, 671–675. [[CrossRef](#)]
49. Li, L.; Qin, X.; Wang, G.; Qi, L.; Du, G.; Hu, Z. Synthesis of anatase TiO₂ nanowires by modifying TiO₂ nanoparticles using the microwave heating method. *Appl. Surf. Sci.* **2011**, *257*, 8006–8012. [[CrossRef](#)]
50. Pimentel, A.; Rodrigues, J.; Duarte, P.; Nunes, D.; Costa, F.M.; Monteiro, T.; Martins, R.; Fortunato, E. Effect of solvents on ZnO nanostructures synthesized by solvothermal method assisted by microwave radiation: A photocatalytic study. *J. Mater. Sci.* **2015**, *50*, 5777–5787. [[CrossRef](#)]
51. Bregadiolli, B.A.; Fernandes, S.L.; Graeff, C.F.O. Easy and fast preparation of TiO₂-based nanostructures using microwave assisted hydrothermal synthesis. *Mater. Res.* **2017**, *20*, 912–919. [[CrossRef](#)]
52. Pimentel, A.; Samouco, A.; Nunes, D.; Araújo, A.; Martins, R.; Fortunato, E. Ultra-fast microwave synthesis of ZnO nanorods on cellulose substrates for UV sensor applications. *Materials* **2017**, *10*, 1308. [[CrossRef](#)]
53. Wang, Y.; Li, L.; Huang, X.; Li, Q.; Li, G. New insights into fluorinated TiO₂ (brookite, anatase and rutile) nanoparticles as efficient photocatalytic redox catalysts. *RSC Adv.* **2015**, *5*, 34302–34313. [[CrossRef](#)]
54. Stagi, L.; Carbonaro, C.M.; Corpino, R.; Chiriu, D.; Ricci, P.C. Light induced TiO₂ phase transformation: Correlation with luminescent surface defects. *Phys. Status Solidi (b)* **2015**, *252*, 124–129. [[CrossRef](#)]
55. Zhang, Q.; Ma, L.; Shao, M.; Huang, J.; Ding, M.; Deng, X.; Wei, X.; Xu, X. Anodic oxidation synthesis of one-dimensional TiO₂ nanostructures for photocatalytic and field emission properties. *J. Nanomater.* **2014**, *2014*, 14. [[CrossRef](#)]
56. Vásquez, G.C.; Peche-Herrero, M.A.; Maestre, D.; Alemán, B.; Ramírez-Castellanos, J.; Cremades, A.; González-Calbet, J.M.; Piqueras, J. Influence of Fe and Al doping on the stabilization of the anatase phase in TiO₂ nanoparticles. *J. Mater. Chem. C* **2014**, *2*, 10377–10385. [[CrossRef](#)]
57. Castellanos-Leal, E.L.; Acevedo-Peña, P.; Güiza-Argüello, V.R.; Córdoba-Tuta, E.M. N and F codoped TiO₂ thin films on stainless steel for photoelectrocatalytic removal of cyanide ions in aqueous solutions. *J. Mater. Res.* **2017**, *20*, 487–495. [[CrossRef](#)]
58. Nezar, S.; Saoula, N.; Sali, S.; Faiz, M.; Mekki, M.; Laoufi, N.; Tabet, N. Properties of TiO₂ thin films deposited by rf reactive magnetron sputtering on biased substrates. *Appl. Surf. Sci.* **2017**, *395*, 172–179. [[CrossRef](#)]
59. Bhandari, S.; Deepa, M.; Srivastava, A.K.; Lakshmikumar, S.T.; RamaKant. Electrochromic response, structure optimization and ion transfer behavior in viologen adsorbed titanium oxide films. *Solid State Ion.* **2009**, *180*, 41–49. [[CrossRef](#)]
60. Nah, Y.-C.; Ghicov, A.; Kim, D.; Schmuki, P. Enhanced electrochromic properties of self-organized nanoporous WO₃. *Electrochem. Commun.* **2008**, *10*, 1777–1780. [[CrossRef](#)]
61. Mjejri, I.; Doherty, C.M.; Rubio-Martinez, M.; Drisko, G.L.; Rougier, A. Double-sided electrochromic device based on metal-organic frameworks. *ACS Appl. Mater. Interfaces* **2017**, *9*, 39930–39934. [[CrossRef](#)]
62. Pereira, S.; Gonçalves, A.; Correia, N.; Pinto, J.; Pereira, L.; Martins, R.; Fortunato, E. Electrochromic behavior of NiO thin films deposited by e-beam evaporation at room temperature. *Sol. Energy Mater. Sol. Cells* **2014**, *120*, 109–115. [[CrossRef](#)]
63. Ramamurthy, V.; Schanze, K.S. *Semiconductor Photochemistry and Photophysics/Volume Ten*; Taylor & Francis: Marcel Dekker, NY, USA, 2003.
64. Barawi, M.; De Trizio, L.; Giannuzzi, R.; Veramonti, G.; Manna, L.; Manca, M. Dual band electrochromic devices based on Nb-doped TiO₂ nanocrystalline electrodes. *ACS Nano* **2017**, *11*, 3576–3584. [[CrossRef](#)]
65. Wen, R.-T.; Niklasson, G.A.; Granqvist, C.G. Eliminating electrochromic degradation in amorphous TiO₂ through Li-Ion detrapping. *ACS Appl. Mater. Interfaces* **2016**, *8*, 5777–5782. [[CrossRef](#)]

